ISSN 1029-9599, Physical Mesomechanics, 2022, Vol. 25, No. 6, pp. 479–491. © The Author(s), 2022. This article is an open access publication.
Russian Text © The Author(s), 2022, published in Fizicheskaya Mezomekhanika, 2022, Vol. 25, No. 4, pp. 5–18.

Micro-, Meso- and Macrostructural Design of Bulk Metallic and Polymetallic Materials by Wire-Feed Electron-Beam Additive Manufacturing

E. A. Kolubaev[1]*, V. E. Rubtsov[1], A. V. Chumaevsky[1], and E. G. Astafurova[1]

[1] *Institute of Strength Physics and Materials Science, Siberian Branch, Russian Academy of Sciences, Tomsk, 634055 Russia*
** e-mail: eak@ispms.ru*

Received May 18, 2022; revised May 18, 2022; accepted May 30, 2022

Abstract—Additive manufacturing of metal materials is one of the most promising technologies in modern industry. A wide variety of current additive manufacturing techniques allow rapid prototyping and industrial production of different-sized products from various structural and functional materials. The structure and physical-mechanical properties of the metal products fabricated by electron-beam additive manufacturing (EBAM) within nonstationary metallurgy in a local molten pool often differ from those of the products fabricated by conventional metallurgy due to different crystallization mechanisms, sequence and completeness of phase transformations, and heterogeneous/homogeneous chemical composition of the resulting material. The possibility to control local metallurgical processes in the molten pool is the key advantage of the EBAM technology. It allows one to control the structure, composition, and properties of mono- and polymetallic, graded, composite and heat-resistant materials in order to obtain products with the desired chemical composition, macroscopic architecture, and microscopic structural parameters. As any new industrial technology, the EBAM method requires the development of scientifically based approaches to the choice of materials and production conditions. Here we provide an overview of the scientific approaches developed for electron-beam additive manufacturing of products from metals and alloys using wire or rods as a feedstock. The range of the studied materials includes additive materials based on copper, bronze, aluminum, nickel, titanium alloys, and different steels, as well as aluminum-based functionally graded materials and copper-based graded materials. The most important research findings are summarized.

Keywords: wire-feed additive manufacturing, metals, alloys, steels, polymetallic components, functionally graded materials

DOI: 10.1134/S1029959922060017

1. INTRODUCTION

Additive manufacturing (or 3D printing) technologies, among which are wire- and powder-based electron beam technologies and their combinations, rest on the use of computer-aided design (CAD) models for rapid layer-by-layer fabrication of products [1–3]. Advances in additive manufacturing of complex metal parts are stimulated by the growing demand for such materials in the aerospace and automotive industries, implant medicine, etc. [1–4]. The undeniable advantage of 3D printing over extractive metallurgy is the possibility of rapid prototyping and fully automatic production of parts of complex shape and various size using CAD models [1–6]. In this regard, additive manufacturing techniques are oriented not to the mass production of structural and functional metal materials, but to the personalized or small-scale production of devices and structural components that are difficult to manufacture, expensive and/or cannot be produced by conventional methods.

The phase composition and mechanical properties of additive materials usually differ from those of their conventionally treated analogues due to the formation of porosity, residual stresses, stress gradient, grain structure and phase composition inhomogeneity, and texture [1–4]. In the current state of the art in the development of additive manufacturing, the key task is not only to obtain a macroscopic product or structure with the desired architecture and properties, but also to search for new scientifically based appro-

aches to controlling the parameters of its microstructure (microstructural design).

There is an explosive increase of global interest in additive technologies, including electron beam technologies. Following this trend, we devoted the past 5 years to intensive development of one of the as yet understudied technology, namely, wire-feed electron-beam additive manufacturing (EBAM).

The final macro- and microstructural parameters, phase composition, and mechanical properties of EBAM objects are determined by the chemical composition and properties of the filament fed to the deposition zone as well as by the conditions in the local molten pool formed by the electron beam. For many materials, an important role is also played by thermal cycling of the already built layers during deposition of the overlying layers. The state of the molten pool can be controlled by varying the electron beam energy and geometry, beam travel rate, geometric conditions and rate of feeding a filament or filaments as well as the heat removal conditions. Thus, the implementation of the microstructural design of EBAM materials is determined by the possibility of precise control over the above technological parameters, which, in turn, depends on the capabilities of the used additive manufacturing facilities. In the past few years, significant progress has been made towards the development of original EBAM equipment and the fabrication of large-sized products (Fig. 1).

For the available additive manufacturing equipment, we developed techniques of feeding the wire filament from mono- (Fig. 2a) and polymetallic (Fig. 2b) materials into the deposition zone as well as for printing with a metal rod for materials that cannot be drawn into wire (Fig. 2c).

The aim of the present paper is to report the scientific findings for electron-beam additive manufacturing of various materials as well as the scientific approaches to the micro-, meso- and macrostructural design of EBAM objects from metallic and polymetallic materials.

Fig. 1. Large-sized products for the aerospace, metallurgical and electrical applications fabricated by the EBAM method from bronze (a), titanium alloy (b), copper (c, d): a—as-built rocket thrust chamber liner; b—as-built part (left) and spherical tank made of two parts (right); c—as-built blast furnace tuyere nose; d—as-built part electrical brush gear holder (color online).

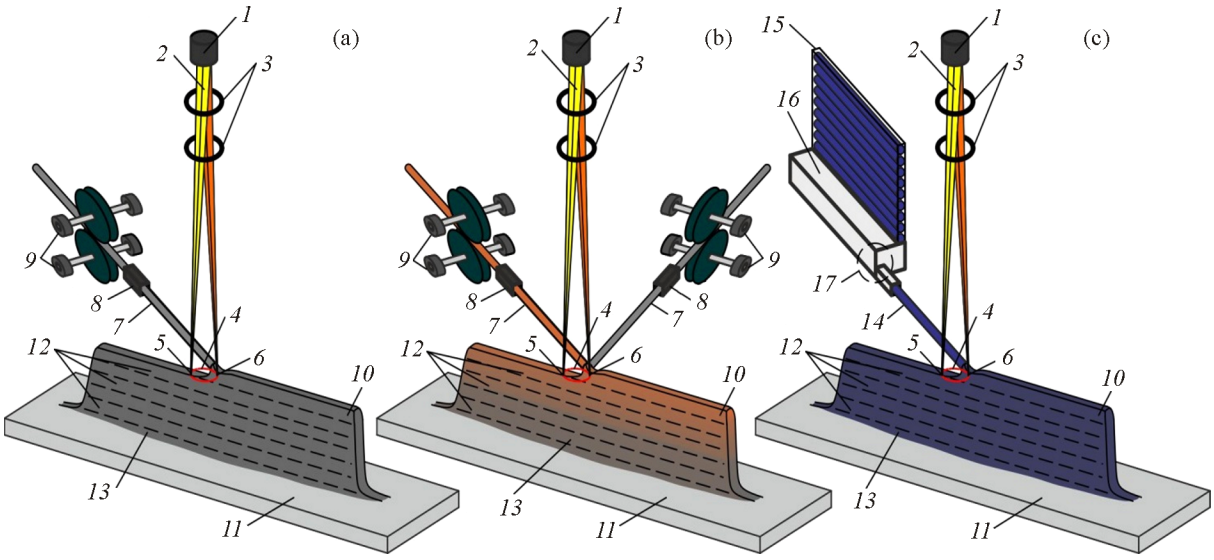

Fig. 2. Schemes of wire-feed electron-beam additive manufacturing of mono- (a) and polymetallic products (b); rod-feed electron-beam additive manufacturing (c): *1*—electron gun, *2*—electron beam, *3*—focusing system, *4*—beam sweep, *5*, *6*—sweep positions on the substrate and on the wire, *7*—wire filament, *8*—tip, *9*—wire feeder, *10*—printed specimen, *11*—substrate, *12*—printed layers, *13*—substrate–specimen transition zone, *14*—rod, *15*—feedstock hopper, *16*—rod feeding system, *17*—rod feeder tip (color online).

2. USE OF EBAM FOR THE GRAIN-BOUNDARY DESIGN OF SPECIMENS FROM COPPER AND BRONZE

Electron-beam additive manufacturing of large-sized products (specimens) from copper and copper alloys is accompanied by the formation of columnar grains in their structure, the long axis of which coincides with the build direction. This conforms to the laws of crystallization during additive manufacturing of many metal materials and causes anisotropy in their mechanical properties [7–9].

When the first layers of copper or bronze (base Cu, 0.4–0.7% Cr, less than 0.3% impurities) are deposited on the Fe-18Cr-9Ni-Ti (mass %) stainless steel substrate, grains grow by the mechanism of collective recrystallization: grain boundaries migrate, resulting in an equilibrium structure with the minimum surface energy and with grains of equal size and shape. As the driving force of collective recrystallization decreases during the process, grains cease to grow on reaching a certain size. Thus, the specimen layers located near the substrate have a microstructure with equiaxed grains about 250 μm in size. In the main part of the specimen, secondary recrystallization ensures the growth of favorably oriented grains and the formation of a crystallographic texture. On completion of secondary recrystallization, abnormally large elongated grains are formed: 3.5 and 0.3 mm in longitudinal and transverse dimensions, respectively (Fig. 3a) [8].

The temperature gradient is a governing factor for morphology and structure of a specimen and determines the mode of crystallization. This fact lies at the basis of the following approach to structure control: the printing process is deliberately stopped after applying n layers of the material to allow the entire build to cool and then restarted. This pause in the EBAM process results in a fine-grained structure in the central part of the specimen, similar to that formed during the deposition of the first copper layers on the substrate (Fig. 3a). Upon resumption of the continuous EBAM process, the directed growth of columnar grains is again observed. Such features of crystallization are caused by the nonuniform heat removal from the build during printing, which can be effectively used to form materials with a macro-, meso-, or microscopically layered structure, in which the anisotropy of mechanical properties will be less pronounced or will be completely removed.

Heat removal has an effect not only on the grain structure of specimens but also can be used for changing the morphology of columnar grains. Specimens of bronze were used to show that, by optimizing the EBAM modes, in particular, by increasing the deposition rate, it is possible to achieve such conditions when a crystallization front in each layer moves

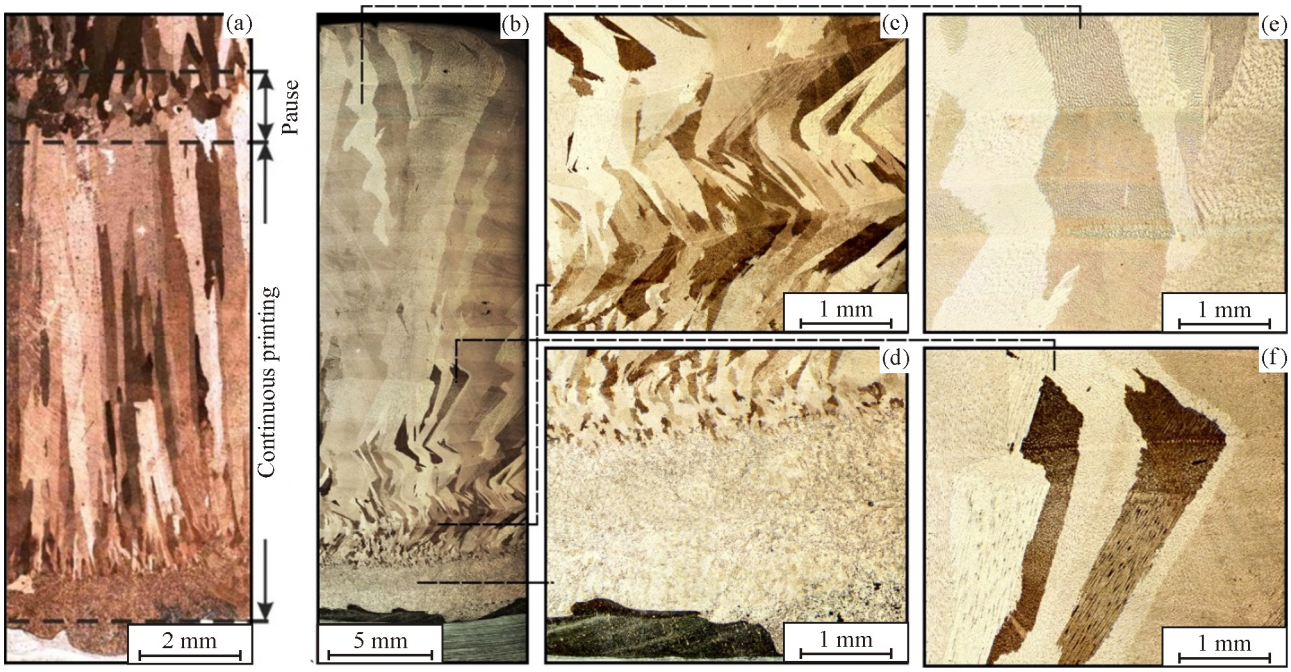

Fig. 3. Macrostructure in the cross section of the copper specimen printed with a pause (a) and formation of zigzag grains in the bronze specimen (b–f): a —copper, b—bronze macrostructure, c—zone with zigzag grains, d—transition zone of finely dispersed structure, e—zone of large dendrites, f—zone with medium dendrites. The pause in the printing process corresponds to the region squared in Fig. 3a (color online).

separately. Under such conditions, a zigzag grain structure is formed in the build direction (Fig. 3b).

The results obtained indicate that the structural design of copper alloys at different levels can be implemented by controlling the crystallization process during the EBAM technology.

3. STRUCTURE CONTROL OF ALUMINUM-MAGNESIUM ALLOYS AT DIFFERENT STRUCTURAL LEVELS

The EBAM method is successfully applied in manufacturing various aluminum alloys, such as 2024 (Al-Cu-Mg), 7075 (Al-Zn-Cu-Mg) [10], 2219 (Al-Cu) [11, 12], and 5356 (Al-Mg) [13, 14]. Printing of bulk products with aluminum-magnesium alloys faces the problems of high porosity of specimens and the reduced content of alloying elements due to their evaporation from the molten pool during printing. The conducted studies show that these problems can be avoided by controlling the heat input to each layer. Analysis was made of how the input heat is related to the microstructure of specimens from alloy AA5356 (base Al, 5.0% Mg, less than 0.4% impurities) as well as to the size and pattern of pore distribution and the concentration of magnesium in them [13]. According to the experimental data, an effective way to eliminate such defects as discontinuities is to remelt the underlying layers of the material during the EBAM process. At low heat input, the depth of a local molten pool formed in the underlying layers during printing is not large enough for all shrinkage cavities and gas pores in the previous layers to get into it. Thus, defects located below the solid-liquid boundary remain in the material. Excessively high heat input causes intensive evaporation of magnesium and formation of large gas pores. The EBAM mode was suggested for alloy AA5356, consisting in the exponential decrease in the electron beam power in layers from the substrate to the upper part of the specimen. This mode enables optimum heat input for maintaining a stable molten pool of the required depth along the entire build height with the minimum evaporation of magnesium. The proposed approach reduces the material porosity by a factor of 4 (from 0.8 to 0.2%) with a decrease in the average pore size from 4 to 1 μm, maintains the magnesium content in the material within the grade composition, and provides the material with the strength 258 MPa and relative elongation 37%, which are typical characteristics for cast alloy AA5356 [13].

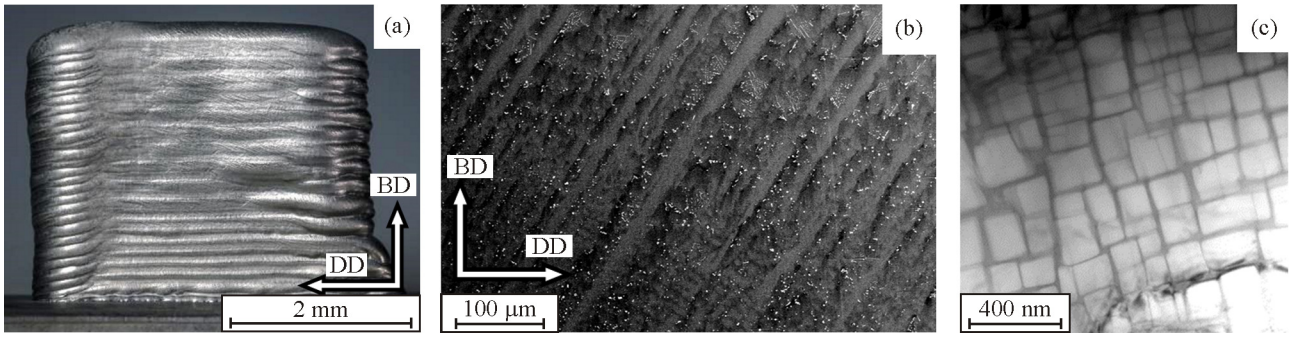

Fig. 4. As-built EBAM part from Ni-based superalloy (a), SEM image of its microstructure with directed dendrites (b), bright-field TEM image of the γ′ phase (c). The arrows indicate the build direction (BD) and the deposition direction (DD).

4. FORMATION OF 3D SPECIMENS FROM HEAT-RESISTANT NICKEL ALLOY

Fabrication of finished products from heat-resistant alloys is a challenge because they are hard to process, have high strength and low plastic characteristics [15, 16]. Additive manufacturing can facilitate a solution to this problem, even with a complex internal architecture. However, production of heat-resistant nickel-based alloys by additive technologies is still a nontrivial task. The rod-based EBAM method was earlier used to fabricate specimens from Ni-based alloy (base Ni, up to 1% Fe, 0.13–0.2% C, up to 0.4% Si, up to 0.4% Mn, 8–9.5% Cr, up to 0.02% Ce, 1.2–2.4% Mo, 9.5–11% W, 9–10.5% Co, 0.8–1.2% Nb, 2–2.9% Ti, 5.1–6% Al, up to 0.04% Zr, up to 0.035% B, less than 0.1% impurities), which were free of cracks and pores at the macro- and microscopic levels (Fig. 4a) [17]. The printing process is schematized in Fig. 2c.

With the exception of the substrate-influenced area and the upper layers unaffected by repeated remelting, heating and cooling, a 3D-printed specimen is represented by directed colonies of dendrites. They grow epitaxially in the build direction with a slope in the deposition direction and cross the macroscopic 3D-printed layers (Fig. 4b). The primary dendrite arm spacing is in the range 20–30 μm, which corresponds to the temperature gradient from 190 to 445 °C/cm [18]. These values of the temperature gradient conform to the conventional casting method with directional crystallization [19]. The predominant orientation of the crystal lattices of the γ and γ′ phases, which are the base of the material [20], along the normal to the substrate surface corresponds to the ⟨001⟩ crystallographic direction.

The fine structure of the material obtained by the EBAM method is similar to that of the cast Ni-based alloy. It consists of cuboidal γ′-phase precipitates of the size 10–100 nm (Fig. 4c) in the γ matrix and submicrocrystalline precipitates of carbides MC and M_6C (where M is Ti, Cr, Nb, Mo, or W) in the interdendritic space. The dimensions of all structural elements of the EBAM material are 1-2 orders of magnitude smaller than those in the cast state. Due to such a structure, the additively manufactured Ni-based alloy has increased mechanical properties over the properties of the cast material (Table 1).

5. STRUCTURE CONTROL OF TITANIUM ALLOY

Titanium alloys are one of the most common choices for additive manufacturing. Titanium-based alloys are widely used in the aviation and aerospace industries, which are currently the main consumers of the EBAM technology [21–25]. Electron-beam additive manufacturing is accompanied by complex ther-

Table 1. Mechanical properties of EBAM specimens from Ni-based alloy rods under uniaxial tension at room temperature in comparison to the cast alloy

Material	σ_B, MPa	$\sigma_{0.2}$, MPa	δ, %
Additive specimen along the dendrite growth direction	1196 ± 38	968 ± 4	12 ± 1
Additive specimen along the build direction	1210 ± 9	1018 ± 21	15 ± 2
Cast specimen	1059 ± 55	776 ± 32	16 ± 2

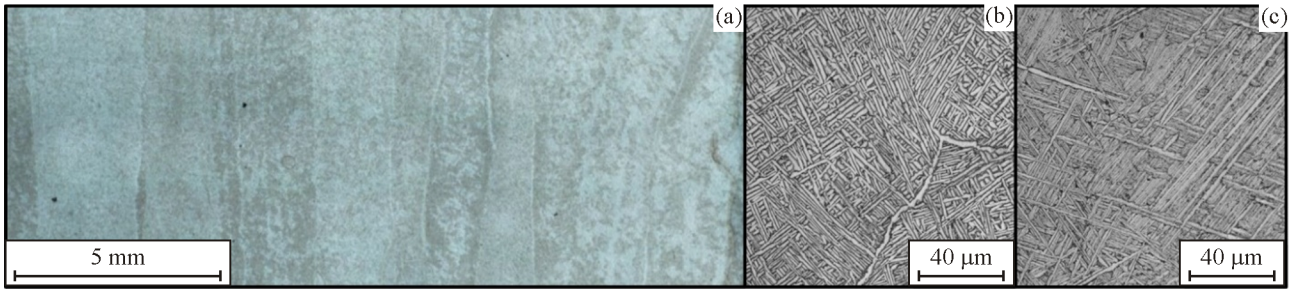

Fig. 5. Macro- (a) and microstructure in the lower (b) and upper (c) parts of the EBAM specimen from titanium alloy (color online).

mal cycling, which, depending on the process parameters, leads to significant anisotropy of properties of products from alloy Ti-6Al-4V [22]. Under various 3D printing conditions, the ultimate strength of the material can vary from 700 to 1200 MPa [23]. Specimens reveal the epitaxial growth of β-phase grains during printing, inside which α(α′)-phase plates are formed after cooling, with dimensions and structure depending on the printing mode [24]. Structures formed in alloy Ti-6Al-4V during EBAM are exemplified in Fig. 5. An increase in the heat removal rate during additive manufacturing, which is implemented by changing the substrate thickness and material, decreases the thickness of the α(α′)-phase plates from 1.1 to 0.8 μm, thus reducing the anisotropy of properties of the alloy from 10 to 5% [24]. The mechanical properties of the EBAM materials are at the same level as those of the corresponding cast alloys (the experimental values are from 578 MPa for large-sized products to 780 MPa for medium-sized products with optimum heat removal) [24].

6. CONTROL OVER STRUCTURE AND PHASE COMPOSITION OF STEELS

Chromium-nickel austenitic stainless steels are most attractive for additive manufacturing [26]. Their good plasticity, weldability, and high corrosion resistance makes them the most favorable structural material all over the world [27]. Of numerous materials used in additive technologies, these steels are high on the list, but scientists and manufacturers come up against some difficulties associated with printing [26, 28–30]. The complex thermal history and nonequilibrium crystallization conditions during the EBAM process contribute to the appearance of such microstructural features in stainless steels as the anisotropy of properties and the formation of a large proportion of δ ferrite. It is possible to reduce or completely suppress the influence of these factors using several scientifically based approaches.

The first approach rests on the stabilization of the austenitic structure of the mentioned steels by using the double-wire-feed EBAM technology (austenitic steel Fe-18Cr-10Ni-Ti-0.08C/nichrome alloy 80% Ni–20% Cr) [31]. The change in the chemical composition of the steel during EBAM (primarily depletion of nickel) is compensated by adding a nickel alloy to the molten pool. This alters the mechanism of steel crystallization and causes a single-phase austenitic state to form immediately after printing. The produced steel (Fe-(19–20)Cr-(15–17)Ni-0.5Mn-0.6Ti-0.7Si-C, mass %) is characterized by not only a single-phase austenitic structure but also, due to a high concentration of nickel, the stability to the strain-induced $\gamma \rightarrow \alpha'$ transformation at room temperature, which is necessary to improve the corrosion properties of the product. This steel has lower strength characteristics but higher ductility compared to two-phase steels obtained by the EBAM method (Table 2).

Another approach is based on the ultrasonic treatment during the EBAM process, which allows for partial suppression of the anisotropy of the grain structure and consequently for improvement of mechanical properties of stainless steels [32]. High-frequency elastic (i.e. ultrasonic) vibrations during nonstationary crystallization processes in metal alloys were previously used in the powder-based additive manufacturing technology to reduce the number of pores and microcracks [33], as well as to refine the microstructure and to improve mechanical properties of stainless steel [34]. Ultrasonic vibrations during the wire-feed EBAM process contribute to grain refinement (the average grain size decreases from 433 ± 145 to 256 ± 17 μm), exert a positive effect on the tensile properties of the material (Table 2), ensure the dissolution and fragmentation of δ-ferrite dendrites, and reduce their volume fraction (from 10 to 8%) [32].

Table 2. Mechanical properties of different steels under uniaxial tension at room temperature

Steel, composition (mass %), and production method		$\sigma_{0.2}$, MPa	σ_B, MPa	δ, %
Cr-Ni-Ti Fe-8.8Ni-17.4Cr-1.1Mn-0.5Ti-0.4Si-0.07C	Cast + SST	315	1050	79
Cr-Ni-Ti Fe-8.8Ni-17.4Cr-1.1Mn-0.5Ti-0.4Si-0.07C	EBAM	216 (BD) 207 (DD)	445 (BD) 510 (DD)	61 (BD) 64 (DD)
Cr-Ni-Ti Fe-8.8Ni-17.4Cr-1.1Mn-0.5Ti-0.4Si-0.07C	EBAM + UT	231 (BD) 233 (DD)	503 (BD) 524 (DD)	70 (BD) 53 (DD)
Cr-Ni Fe-9.1Ni-19.1Cr-0.95Si-0.12C	EBAM	245–264 (BD) 252–305 (DD)	820–855 (BD) 810–890 (DD)	43–47 (BD) 36–45 (DD)
AISI 321 + NiCr Fe-(19–20)Cr-(15–17)Ni-0.5Mn-0.6Ti-0.7Si-C	Double-wire-feed EBAM	148 (BD)	375 (BD)	54 (BD)
Cr-Ni-Nb Fe-9.5Ni-18.7Cr-1.6Mn-0.1C-0.7Si-1.4Nb	EBAM	235 (BD)	800 (BD)	32 (BD)
Cr-Mn-V-N Fe-21.6Cr-25.7Mn-1.4V-0.7C-1.2N	Cast + SST	843	1419	28
Cr-Mn-V-N Fe-22.3Cr-19.9Mn-1.4V-0.69C-1.16N	EBAM	878 (BD)	1306 (BD)	2 (BD)
Cr-Mn-N Fe-20.7Cr-22.2Mn-0.3Ni-0.6Si-0.15C-0.53N	Cast + SST	510	914	38
Cr-Mn-N Fe-22.9Cr-10.8Mn-0.1Ni-0.6Si-0.1C-0.48N	EBAM	440–470 (BD) 527–555 (DD)	775–857 (BD) 864–879 (DD)	28–40 (BD) 48–50 (DD)
Low-carbon steel Fe-(1.8–2.1)Mn-(0.7–0.95)Si-(0.05–0.11)C	Cast + SST	334	491	38
Low-carbon steel Fe-(1.3–1.7)Mn-(0.5–0.8)Si-<0.12C	EBAM	245–280 (BD) 273–339 (DD)	439–445 (BD) 430–464 (DD)	28–32 (BD) 25–37 (DD)

BD—properties in the build direction, DD—properties in the deposition direction, SST—solid solution treatment, UT—ultrasonic treatment. The derived data are compared to those of the conventionally treated analogues.

As for austenitic steels, the EBAM method was effectively used to produce 3D specimens of high-nitrogen steels [35, 36]. This approach suggests that the use of nitrogen as an alloying element stabilizes the austenitic phase and removes nickel from the steel composition, improves its strength properties by forming an interstitial solid solution on retention of plasticity and fracture toughness. The prerequisites for these studies were works reporting the positive effect of nitrogen on the mechanical properties of additively manufactured bulk materials [37–39]. The EBAM method was used to produce specimens from chromium-manganese steels with the interstitial atom concentrations 0.5 and 1.9 mass % [35, 36]. It was found that these specimens lose manganese during additive manufacturing, but retain the initially high concentration of interstitial atoms.

Products from high-nitrogen chromium-manganese steel were successfully fabricated by the EBAM method using rods from high-nitrogen steel Fe-20.7Cr-22.2Mn-0.3Ni-0.6Si-0.15C-0.53N (mass %). The produced specimens had a dual-phase structure (austenite–40% ferrite) of dendritic morphology. The high volume fraction of ferrite and the dendritic microstructure of the steel were due to a decrease in the manganese concentration from 22 to 11 mass % during additive manufacturing and a change in the mechanism of steel solidification. The total concentration of interstitial atoms (≈0.5 mass %) changed insignificantly during the EBAM process. The predominant formation of austenitic dendrites with a high content of nitrogen (about 0.9 mass %) at the early stages of solidification led to depletion of the melt in respect of nitrogen and manganese, which resulted in the formation of nitrogen-free ferrite in the interdendritic space. Despite a significant change in the elemental and phase composition of the EBAM steel, its mechanical properties were comparable to those of the austenitic steel used as the feedstock for additive manufacturing (Table 2).

In printing with steel rods of the composition Fe-21.6Cr-25.7Mn-1.4V-0.7C-1.2N, the decreased concentration of manganese did not cause destabilization of the austenitic structure, and the fabricated products

had a heterophase structure based on austenite with dispersed phases of different composition and morphology (chromium and vanadium carbonitrides, intermetallic compounds (Fe, Cr, Mn, V)) [36]. The complex effect of solid-solution strengthening and precipitation strengthening determines high strength properties of the additively manufactured high-nitrogen vanadium-containing austenitic steel, though its plasticity is not high due to the formation of dispersed phases (Table 2).

Additive technologies allow the production of bulk products from ferritic and ferritic-pearlitic steels, though this area of research is still poorly developed, and there are still few works in the modern literature devoted to the study of the structure and properties of such materials [40–42]. The EBAM method was used to fabricate steel products from the wire of low-carbon steel Fe-2Mn-1Si-0.1C [43]. Their structure consisted of nonequiaxed ferrite grains hundreds of micrometers in size, but columnar grains elongated in the build direction did not form (as with austenitic steels). The additively manufactured steel had a volume-constant phase composition but different morphology of ferrite grains. Quasi-equiaxed ferrite grains with coarse spherical carbides predominated in the lower part of the specimen. Its central and upper parts contained not only nonequiaxed ferrite grains with carbides but also grains with a lamellar ferrite morphology, which resembles martensite or bainite. Thus, multiple thermal cycles and heating of the material during the EBAM process resulted in different sequences of phase transformations in different parts of the specimen. This caused the formation of a noticeable anisotropy of mechanical properties of such steel, but in general, its mechanical characteristics were not inferior to its analogue obtained by conventional methods of casting and heat treatment (normalization) (Table 2).

7. DESIGN OF FUNCTIONALLY GRADED MATERIALS BASED ON ALUMINUM, COPPER, AND STAINLESS STEEL

At present, there is an increasing demand for functionally graded materials, which possess the properties of dissimilar materials combined into a single macroscopic object with a gradient variation in composition, structure, and properties [44, 45]. The problem of formation of bonding layers in functionally graded materials is manly associated with low or zero mutual solubility of their components, heterogeneity of their structures, and the tendency to form brittle intermetallic phases [44–47].

Functionally graded materials were produced from aluminum alloys with different functional properties: alloy AA4047 (base Al, 11–13% Si, 0.6% Fe, 0.15% Ti, 0.2% Zn, 0.05% Cu) with good casting properties and corrosion resistance, high-strength alloy AA7075 (base Al, 5.6–6.1% Zn, 2.1–2.5% Mg, 1.2–1.6% Cu, less than 0.5% impurities), and high-strength and corrosion-resistant alloy AA5356 (base Al, 5.0% Mg, less than 0.4% impurities).

Aluminum-based functionally graded materials were produced by the EBAM methods from AA4047 alloy on the alloy AA7075 substrate [46] and from alloy AA5356 on the alloy AA7075 substrate [47]. The transition zone formed between alloys AA4047 and AA7075 during the EBAM process had a sharp interface. It was enriched in silicon and contained particles of the Mg_2Si phase, which reduced the corrosion properties of the gradient layers from those of alloy AA4047 [46]. The functionally graded material based on aluminum alloys AA5356 and AA7075 was characterized by the formation of second-phase particles of various compositions at the interface, which increase the hardness and strength of the transition zone. The investigation of the corrosion resistance of the fabricated material revealed intergranular corrosion in the lower part of the transition zone due to the formation of particles depleted of iron. Its value decreased as the region with the alloy AA5356 composition was approached, where pitting corrosion was observed due to the formation of Mg_2Si particles during printing.

The EBAM process is also capable of producing bimetallic steel-copper functionally graded materials [48]. The investigated bimetallic specimens exhibited a microstructural variation throughout the height. In the austenitic steel part of the specimen, the gradient zone starts with the structure represented by copper inclusions within austenitic grains and along their boundaries (Figs. 6a, 6b). As the copper part of the specimen is approached, the structure becomes cross-linked with copper inclusions along the boundaries of dendrites or grains (Figs. 6c–6e) and then gives way to regions with iron inclusions in copper grains (Fig. 6f). The solubility of copper in the γ-phase lattice (in the steel part of the graded material) and of steel elements in the copper part agrees with the phase diagrams for Fe-Cu systems and to a large extent determines the material structure in the gradient zone [48].

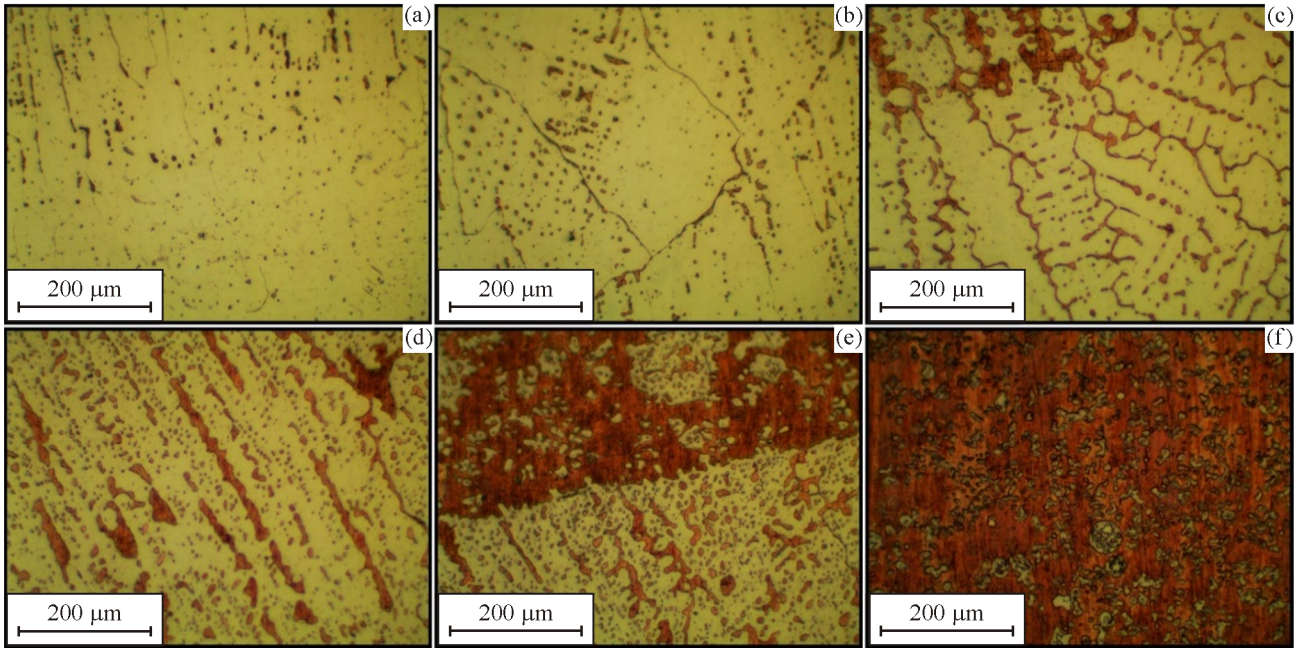

Fig. 6. Metallographic images of the lower (a, b), central (c–e) and upper (f) parts of the bimetallic copper-stainless steel functionally graded specimen [48] (color online).

8. FORMATION OF METAL-MATRIX COMPOSITE MATERIALS

Additive manufacturing of wear-resistant metal-matrix composites is a field of extensive research [49–51]. Composites of the CuAl-B_4C system with the gradient distribution of particles were obtained by the combined technology of wire-feed and powder-bed EBAM [52]. Specimens were formed using $CuAl_7$ wire and $(B_4C)_{0.25}Al_{0.75}$ and $(B_4C)_{0.5}Al_{0.5}$ powder mixtures as feedstock. In each case, 0.8-mm-thick composite layers were deposited on the $CuAl_7$ alloy substrate. A detailed structural analysis of the specimens indicated a nonuniform distribution of B_4C particles in the material (Fig. 7), which is due to

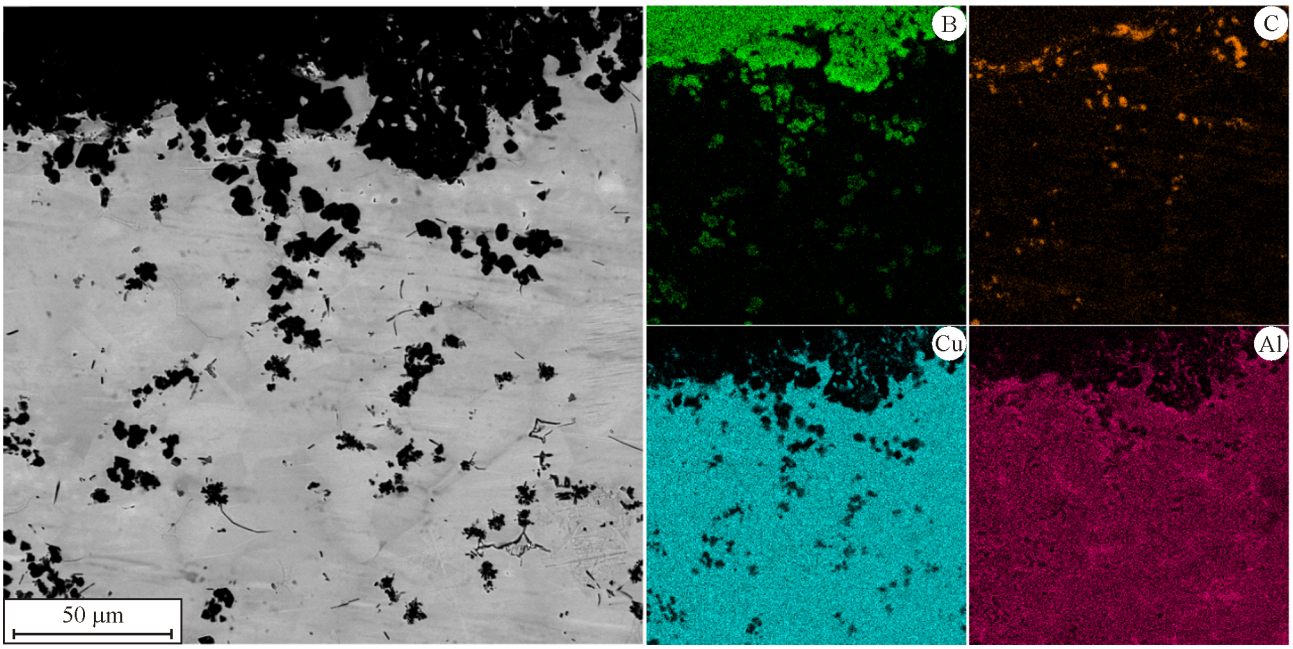

Fig. 7. SEM images and element distribution maps (X-ray microanalysis technique) in cross sections of CuAl-B_4C metal-matrix composite specimens (color online).

the redistribution (floating) of particles during remelting of the previously printed layer [52].

Friction tests on the resulting metal-matrix composites at room temperature showed that reinforcement of the bronze matrix with B_4C particles increases the wear resistance of aluminum bronze: the friction coefficient decreases from 0.26 to 0.19. The wear resistance of the composite printed using the $(B_4C)_{0.25}Al_{0.75}$ powder is 2.2 times higher than that using the $(B_4C)_{0.5}Al_{0.5}$ powder, which is explained by lower abrasive wear due to a smaller number of B_4C particles [51].

9. CONCLUSIONS

In the last 5 years significant progress was made towards the creation and improvement of equipment for electron-beam additive manufacturing of metal and composite materials. Scientifically based approaches were developed to control the structure, composition, and various functional properties of industrially important metals and alloys. As a result, copper, bronze, aluminum, nickel, titanium alloys, various steels, functionally graded materials, and metal-matrix composites were successfully produced by the EBAM technology. The properties of the produced materials are slightly inferior, and often even superior, to those of their analogues obtained by conventional metallurgy, which increases the prospect of using additive manufactured materials in industry.

FUNDING

The work was carried out at the Laboratory of Local Metallurgy in Additive Technologies, the Laboratory for Quality Control in Materials and Structures, and the Laboratory of Physics of Hierarchical Structures in Metals and Alloys of the ISPMS SB RAS within the government statement of work for ISPMS SB RAS, research lines FWRW-2022-0004 and FWRW-2022-0005.

ACKNOWLEDGMENTS

The authors are grateful to Cand. Sci. (Phys.-Math.) S.V. Astafurov, Cand. Sci. (Eng.) A.V. Vorontsov, Cand. Sci. (Eng.) D.A. Guryanov, A.V. Gusarova, Cand. Sci. (Phys.-Math.) A.P. Zykova, Cand. Sci. (Eng.) T.A. Kalashnikova, K.N. Kalashnikov, Yu.V. Kushnarev, Cand. Sci. (Phys.-Math.) G.G. Maier, E.V. Melnikov, V.A. Moskvina, Cand. Sci. (Phys.-Math.) E.N. Moskvichev, Cand. Sci. (Phys.-Math.) S.Yu. Nikonov, K.S. Osipovich, M.Yu. Panchenko, K.A. Reunova, Dr. Sci. (Eng.) S.Yu. Tarasov, Cand. Sci. (Eng.) A.V. Filippov, Cand. Sci. (Phys.-Math.) S.V. Fortuna, N.N. Shamarin, and V.R. Utyaganova for help in producing materials and conducting experimental studies.

OPEN ACCESS

REFERENCES

1. Ding, D., Pan, Z., Cuiuri, D., and Li, H., Wire-Feed Additive Manufacturing of Metal Components: Technologies, Developments and Future Interests, *Int. J. Adv. Manuf. Technol*., 2015, vol. 81, pp. 465–481. https://doi.org/10.1007/s00170-015-7077-3
2. Frazier, W.E., Metal Additive Manufacturing: A Review, *J. Mater. Eng. Perform*., 2014, vol. 23, pp. 1917–1928. https://doi.org/10.1007/s11665-014-0958-z
3. DebRoy, T., Wei, H.L., Zuback, J.S., Mukherjee, T., Elmer, J.W., Milewski, J.O., Beese, A.M., Wilson-Heid, A., De, A., and Zhang, W., Additive Manufacturing of Metallic Components—Process, Structure and Properties, *Progr. Mater. Sci*., 2018, vol. 92, pp. 112–224. https://doi.org/10.1016/j.pmatsci.2017.10.001
4. Li, N., Huang, S., Zhang, G., Qin, R., Liu, W., Xiong, H., Shi, G., and Blackburn, J., Progress in Additive Manufacturing on New Materials: A Review, *J. Mater. Sci. Technol*., 2019, vol. 35, pp. 242–269. https://doi.org/10.1016/j.jmst.2018.09.002
5. Blakey-Milner, B., Gradl, P., Snedden, G., Brooks, M., Pitot, J., Lopez, E., Leary, M., Berto, F., and du Plessis, A., Metal Additive Manufacturing in Aerospace: A Review, *Mater. Des*., 2021, vol. 209, p. 110008. https://doi.org/10.1016/j.matdes.2021.110008
6. Calignano, F., Manfredi, D., Ambrosio, E.P., Biamino, S., Lombardi, M., Atzeni, E., Salmi, A., Minetola, P., Iuliano, L., and Fino, P., Overview on Additive

Manufacturing Technologies, *Proc. IEEE*, 2017, vol. 105(4), no. 7803596, pp. 593–612. https://doi.org/10.1109/JPROC.2016.2625098
7. Åkerfeldt, P., Antti, M.L., and Pederson, R., Influence of Microstructure on Mechanical Properties of Laser Metal Wire-Deposited Ti-6Al-4V, *Mater. Sci. Eng. A*, 2016, vol. 674, pp. 428–437. https://doi.org/10.1016/j.msea.2016.07.038
8. Rago, I., Iannone, M., Marra, F., Bracciale, M.P., Paglia, L., Orlandi, D., Cortis, D., and Pettinacci, V., 3D-Printed Pure Copper: Density and Thermal Treatments Effects, *Lect. Notes Mech. Eng*., 2022, pp. 721–728. https://doi.org/10.1007/978-3-030-91234-5
9. Wang, Y., Chen, X., Konovalov, S., Su, C., Siddiquee, A.N., and Gangil, N., In-Situ Wire-Feed Additive Manufacturing of Cu-Al Alloy by Addition of Silicon, *Appl. Surf. Sci*., 2019, vol. 487, pp. 1366–1375. https://doi.org/10.1016/j.apsusc.2019.05.068
10. Mahale, T., Cormier, D., Harrysson, O., and Ervin, K., Advances in Electron Beam Melting of Aluminum Alloys, in *18th Solid Free. Fabr. Symp. SFF 2007*, 2007, pp. 312–323. http://dx.doi.org/10.26153/tsw/7216
11. Domack, M.S., Taminger, K.M., and Begley, M., Metallurgical Mechanisms Controlling Mechanical Properties of Aluminium Alloy 2219 Produced by Electron Beam Freeform Fabrication, *Mater. Sci. Forum*, 2006, vol. 519–521, pp. 1291–1296. https://doi.org/10.4028/www.scientific.net/MSF.519-521.1291
12. Taminger, K.M., Hafley, R.A., and Domack, M.S., Evolution and Control of 2219 Aluminum Microstructural Features Through Electron Beam Freeform Fabrication, *Mater. Sci. Forum*, 2006, vol. 519–521, pp. 1297–1304. https://doi.org/10.4028/www.scientific.net/MSF.519-521.1297
13. Utyaganova, V.R., Filippov, A.V., Shamarin, N.N., Vorontsov, A.V., Savchenko, N.L., Fortuna, S.V., Gurianov, D.A., Chumaevskii, A.V., Rubtsov, V.E., and Tarasov, S.Y., Controlling the Porosity Using Exponential Decay Heat Input Regimes during Electron Beam Wire-Feed Additive Manufacturing of Al-Mg Alloy, *Int. J. Adv. Manuf. Technol*., 2020, vol. 108(9), pp. 2823–2838. https://doi.org/10.1007/s00170-020-05539-9
14. Eliseev, A.A., Utyaganova, V.R., Vorontsov, A.V., Ivanov, V.V., Rubtsov, V.E., and Kolubaev, E.A., Comparative Analysis of Structure and Mechanical Properties of Additive Objects Manufactured by Electron Beam Method and Cold Metal Transfer, *Russ. J. Non-Ferr. Met*., 2020, vol. 61(5), pp. 517–522. https://doi.org/10.3103/S106782122005003X
15. Li, Y., Liang, X., Yu, Y., Wang, D., and Lin, F., Review on Additive Manufacturing of Single-Crystal Nickel-Based Superalloys, *Chin. J. Mech. Eng. Add. Manuf. Front*., 2022, vol. 1(1), p. 100019. https://doi.org/10.1016/j.cjmeam.2022.100019
16. Shahwaz, M., Nath, P., and Sen, I., A Critical Review on the Microstructure and Mechanical Properties Correlation of Additively Manufactured Nickel-Based Superalloys, *J. Alloys Compd.*, 2022, vol. 907, p. 164530. https://doi.org/10.1016/j.jallcom.2022.164530
17. Fortuna, S.V., Gurianov, D.A., Kalashnikov, K.N., Chumaevskii, A.V., Mironov, Yu.P., and Kolubaev, E.A., Directional Solidification of a Nickel-Based Superalloy Product Structure Fabricated on Stainless Steel Substrate by Electron Beam Additive Manufacturing, *Metall. Mater. Trans. A*, 2021, vol. 52, pp. 857–870. https://doi.org/10.1007/s11661-020-06090-8
18. Zhang, Y., Huang, B., and Li, J., Microstructural Evolution with a Wide Range of Solidification Cooling Rates in a Ni-Based Superalloy, *Metall. Mater. Trans. A*, 2013, vol. 44(4), pp. 1641–1644. https://doi.org/10.1007/s11661-013-1645-7
19. Wang, H., Zhang, X., Meng, J., Yang, J., Yang, Y., Zhou, Y., and Sun, X., A New Model of Competitive Grain Growth Dominated by the Solute Field of the Nickel-Based Superalloys during Directional Solidification, *J. Alloys Compd.*, 2021, vol. 873, p. 159794. https://doi.org/10.1016/j.jallcom.2021.159794
20. Shahwaz, M., Nath, P., and Sen, I., A Critical Review on the Microstructure and Mechanical Properties Correlation of Additively Manufactured Nickel-Based Superalloys, *J. Alloys Compd.*, 2022, vol. 907, p. 164530. https://doi.org/10.1016/j.jallcom.2022.164530
21. Peters, M., Kumpfert, J., Ward, C.H., and Leyens, C., Titanium Alloys for Aerospace Applications, *Adv. Eng. Mater*., 2003, vol. 5(6), pp. 419–427. https://doi.org10.1002/adem.200310095
22. Carroll, B.E., Palmer, T.A., and Beese, A.M., Anisotropic Tensile Behavior of Ti–6Al–4V Components Fabricated with Directed Energy Deposition Additive Manufacturing, *Acta Mater.*, 2015, vol. 87, pp. 309–320. https://doi.org/10.1016/j.actamat.2014.12.054
23. Liu, S. and Shin, Y.C., Additive Manufacturing of Ti6Al4V Alloy: A Review, *Mater. Des*., 2019, vol. 164, p. 107552. https://doi.org/10.1016/j.matdes.2018.107552
24. Kalashnikov, K.N., Chumaevskii, A.V., Kalashnikova, T.A., and Kolubaev, E.A., A Substrate Material and Thickness Influence on the 3D-Printing of Ti–6Al–4V Components Via Wire-Feed Electron Beam Additive Manufacturing, *J. Mater. Res. Technol*., 2022, vol. 16, pp. 840–852. https://doi.org/10.1016/j.jmrt.2021.12.024
25. Panin, A.V., Kazachenok, M.S., Perevalova, O.B., Sinyakova, E.A., Krukovsky, K.V., and Martynov, S.A., Multiscale Deformation of Commercial Titanium and Ti–6Al–4V Alloy Subjected to Electron Beam Surface Treatment, *Phys. Mesomech*., 2018, vol. 21, no. 5, pp. 441–451. https://doi.org/10.1134/S1029959918050089
26. Bajaj, P., Hariharan, A., Kini, A., Kürnsteiner, P., Raabe, D., and Jägle, E.A., Steels in Additive Manufacturing: A Review of Their Microstructure and Proper-

ties, *Mater. Sci. Eng. A*, 2020, vol. 772, p. 138633. https://doi.org/10.1016/j.msea.2019.138633
27. Bhadeshia, H. and Honeykombe, R., *Steels: Microstructure and Properties*, Amsterdam, Netherlands: Elsevier, 2006.
28. Kurzynowski, T., Gruber, K., Stopyra, W., Kuźnicka, B., and Chlebus, E., Correlation between Process Parameters, Microstructure and Properties of 316L Stainless Steel Processed by Selective Laser Melting, *Mater. Sci. Eng. A*, 2018, vol. 718, pp. 64–73. https://doi.org/10.1016/j.msea.2018.01.103
29. Wang, Z., Palmer, T.A., and Beese, A.M., Effect of Processing Parameters on Microstructure and Tensile Properties of Austenitic Stainless Steel 304L Made by Directed Energy Deposition Additive Manufacturing, *Acta Mater*., 2016, vol. 110, pp. 226–235. https://doi.org/10.1016/j.actamat.2016.03.019
30. Wang, L., Xue, J., and Wang, Q., Correlation between Arc Mode, Microstructure, and Mechanical Properties during Wire Arc Additive Manufacturing of 316L Stainless Steel, *Mater. Sci. Eng. A*, 2019, vol. 751, pp. 183–190. https://doi.org/10.1016/j.msea.2019.02.078
31. Moskvina, V.A., Melnikov, E.V., Astafurov, S.V., Panchenko, M.Yu., Reunova, K.A., Kolubaev, E.A., and Astafurova, E.G., Stable High-Nickel Austenitic Steel Produced by Electron Beam Additive Manufacturing Using Dual Wire-Feed System, *Mater. Lett*., 2021, vol. 305, p. 130863. https://doi.org/10.1016/j.matlet.2021.130863
32. Vorontsov, A., Astafurov, S., Melnikov, E., Moskvina, V., Kolubaev, E., and Astafurova, E., The Microstructure, Phase Composition and Tensile Properties of Austenitic Stainless Steel in a Wire-Feed Electron Beam Melting Combined with Ultrasonic Vibration, *Mater. Sci. Eng. A*, 2021, vol. 820, p. 141519. https://doi.org/10.1016/j.msea.2021.141519
33. Ning, F. and Cong, W., Microstructures and Mechanical Properties of Fe-Cr Stainless Steel Parts Fabricated by Ultrasonic Vibration-Assisted Laser Engineered Net Shaping Process, *Mater. Lett*., 2016, vol. 179, pp. 61–64. https://doi.org/10.1016/j.matlet.2016.05.055
34. Todaro, C.J., Easton, M.A., Qiu, D., Brandt, M., StJohn, D.H., and Qian, M., Fine-Grained Stainless Steel by Ultrasound-Assisted Additive Manufacturing, *Addit. Manuf*., 2020, p. 101632. https://doi.org/10.1016/j.addma.2020.101632
35. Astafurov, S., Astafurova, E., Reunova, K., Melnikov, E., Panchenko, M., Moskvina, V., Maier, G., Rubtsov, V., and Kolubaev, E., Electron-Beam Additive Manufacturing of High-Nitrogen Steel: Microstructure and Tensile Properties, *Mater. Sci. Eng. A*, 2021, vol. 826, p. 141951. https://doi.org/10.1016/j.msea.2021.141951
36. Astafurova, E.G., Astafurov, S.V., Reunova, K.A., Melnikov, E.V., Moskvina, V.A., Panchenko, M.Yu., Maier, G.G., Rubtsov, V.E., and Kolubaev, E.A., Structure Formation in Vanadium-Alloyed Chromium-Manganese Steel with a High Concentration of Interstitial Atoms C + N = 1.9 wt % during Electron-Beam Additive Manufacturing, *Phys. Mesomech*., 2022, vol. 25, no. 1, pp. 1–11. https://doi.org/10.1134/S1029959922010015
37. Zhang, X., Zhou, Q., Wang, K., Peng, Y., Ding, J., Kong, J., and Williams, S., Study on Microstructure and Tensile Properties of High Nitrogen Cr-Mn Steel Processed by CMT Wire and Arc Additive Manufacturing, *Mater. Des*., 2019, vol. 166, p. 107611. https://doi.org/10.1016/j.matdes.2019.107611
38. Panin, V.E., Narkevich, N.A., Durakov, V.G., and Shulepov, I.A., Control of the Structure and Wear Resistance of a Carbon-Nitrogen Austenitic Steel Coating Produced by Electron Beam Cladding, *Phys. Mesomech*., 2021, vol. 24, no. 1, pp. 53–60. https://doi.org/10.1134/S1029959921010082
39. Boes, J., Röttger, A., and Theisen, W., Microstructure and Properties of High-Strength C + N Austenitic Stainless Steel Processed by Laser Powder Bed Fusion, *Addit. Manuf*., 2020, vol. 32, p. 101081. https://doi.org/10.1016/j.addma.2020.101081
40. Li, Y., Wu, S., Li, H., and Cheng, F., Dramatic Improvement of Impact Toughness for the Fabricating of Low-Carbon Steel Components Via Submerged Arc Additive Manufacturing, *Mater. Lett*., 2021, vol. 283, p. 128780. https://doi.org/10.1016/j.matlet.2020.128780
41. Ahsan, Md.R.U., Tanvir, A.N.M., Seo, G.-J., Bates, B., Hawkins, W., Lee, C., Liaw, P.K., Noakes, M., Nycz, A., and Kim, D.B., Heat-Treatment Effects on a Bimetallic Additively-Manufactured Structure (BAMS) of the Low-Carbon Steel and Austenitic-Stainless Steel, *Addit. Manuf.*, 2020, vol. 32, p. 101036. https://doi.org/10.1016/j.addma.2020.101036
42. Sun, L., Jiang, F., Huang, R., Yuan, D., Guo, C., and Wang, J., Anisotropic Mechanical Properties and Deformation Behavior of Low-Carbon High-Strength Steel Component Fabricated by Wire and Arc Additive Manufacturing, *Mater. Sci. Eng. A*, 2020, vol. 787, p. 139514. https://doi.org/10.1016/j.msea.2020.139514
43. Astafurova, E.G., Melnikov, E.V., Astafurov, S.V., Panchenko, M.Yu., Reunova, K.A., Moskvina, V.A., Maier, G.G., and Kolubaev, E.V., Microstructure and Mechanical Properties of Low-Carbon Steel Fabricated by Electron-Beam Additive Manufacturing, *Lett. Mater*., 2021, vol. 11, no. 4, pp. 427–432. https://doi.org/10.22226/2410-3535-2021-4-427-432
44. Kim, D., Park, K., Chang, M., Joo, S., Hong, S., Cho, S., and Kwon, H., Fabrication of Functionally Graded Materials Using Aluminum Alloys Via Hot Extrusion, *Metals*, 2019, vol. 9(2), p. 210. https://doi.org/10.3390/met9020210
45. Owoputi, A.O., Inambao, F.L., and Ebhota, W.S., A Review of Functionally Graded Materials: Fabrication Processes and Applications, *Int. J. Appl. Eng. Res*.,

2018, vol. 13(23), pp. 16141–16151. http://www.ripublication.com/ijaer18/ijaerv13n23_01.pdf

46. Filippov, A.V., Utyaganova, V.R., Shamarin, N.N., Vorontsov, A.V., Savchenko, N.L., Gurianov, D.A., Chumaevskii, A.V., Rubtsov, V.E., Kolubaev, E.A., and Tarasov, S.Y., Microstructure and Corrosion Resistance of AA4047/AA7075 Transition Zone Formed Using Electron Beam Wire-Feed Additive Manufacturing, *Materials*, 2021, vol. 14(22), p. 6931. https://doi.org/10.3390/ma14226931
47. Utyaganova, V.R., Filippov, A.V., Tarasov, S.Y., Shamarin, N.N., Gurianov, D.A., Vorontsov, A.V., Chumaevskii, A.V., Fortuna, S.V., Savchenko, N.L., Rubtsov, V.E., and Kolubaev, E.A., Characterization of AA7075/AA5356 Gradient Transition Zone in an Electron Beam Wire-Feed Additive Manufactured Sample, *Mater. Charact*., 2021, vol. 172, p. 110867. https://doi.org/10.1016/j.matchar.2020.110867
48. Osipovich, K., Astafurova, E., Chumaevskii, A., Kalashnikov, K., Astafurov, S., Maier, G., Melnikov, E., Moskvina, V., Panchenko, M., Tarasov, S., Rubtsov, V., and Kolubaev, E., Gradient Transition Zone Structure in "Steel–Copper" Sample Produced by Double Wire-Feed Electron Beam Additive Manufacturing, *J. Mater. Sci*., 2020, vol. 55, pp. 9258–9272. https://doi.org/10.1007/s10853-020-04549-y
49. Wang, Q.Z., Lin, X., Kang, N., Wen, X.L., Cao, Y., Lu, J.L., Peng, D.J., Bai, J., Zhou, Y.X., El Mansori, M., and Huang, W.D., Effect of Laser Additive Manufacturing on the Microstructure and Mechanical Properties of TiB_2 Reinforced Al-Cu Matrix Composite, *Mater. Sci. Eng. A*, 2022, vol. 840, p. 142950. https://doi.org/10.1016/j.msea.2022.142950
50. Zhang, X., Li, L., and Liou, F., Additive Manufacturing of Stainless Steel—Copper Functionally Graded Materials Via Inconel 718 Interlayer, *J. Mater. Res. Technol*., 2021, vol. 15, pp. 2045–2058. https://doi.org/10.1016/j.jmrt.2021.09.027
51. Feenstra, D.R., Banerjee, R., Fraser, H.L., Huang, A., Molotnikov, A., and Birbilis, N., Critical Review of the State of the Art in Multi-Material Fabrication Via Directed Energy Deposition, *Curr. Opin. Solid. St. M*., 2021, vol. 25(4), p. 100924. https://doi.org/10.1016/j.cossms.2021.100924
52. Filippov, A.V., Khoroshko, E.S., Shamarin, N.N., Savchenko, N.L., Moskvichev, E.N., Utyaganova, V.R., Kolubaev, E.A., Smolin, A.Yu., and Tarasov, S.Yu., Characterization of Gradient CuAl–B_4C Composites Additively Manufactured Using a Combination of Wire-Feed and Powder-Bed Electron Beam Deposition Methods, *J. Alloys Compd.*, 2021, vol. 859, p. 157824. https://doi.org/10.1016/j.jallcom.2020.157824